Density and anomalous thermal expansion of deeply cooled water confined in mesoporous silica investigated by synchrotron X-ray diffraction

Kao-Hsiang Liu, Yang Zhang, Jey-Jau Lee, Chia-Cheng Chen, Yi-Qi Yeh, Sow-Hsin Chen, and Chung-Yuan Mou

Citation: The Journal of Chemical Physics **139**, 064502 (2013); doi: 10.1063/1.4817186
View online: http://dx.doi.org/10.1063/1.4817186
View Table of Contents: http://scitation.aip.org/content/aip/journal/jcp/139/6?ver=pdfcov
Published by the AIP Publishing

This article is copyrighted as indicated in the abstract. Reuse of AIP content is subject to the terms at: http://scitation.aip.org/termsconditions. Downloaded to IP: 140.110.200.123 On: Mon, 25 Nov 2013 06:41:17

Density and anomalous thermal expansion of deeply cooled water confined in mesoporous silica investigated by synchrotron X-ray diffraction

Kao-Hsiang Liu,[1,2] Yang Zhang,[3] Jey-Jau Lee,[4] Chia-Cheng Chen,[1] Yi-Qi Yeh,[1,4] Sow-Hsin Chen,[2] and Chung-Yuan Mou[1,a)]

[1]*Department of Chemistry, National Taiwan University, Taipei 106, Taiwan*
[2]*Department of Nuclear Science and Engineering, Massachusetts Institute of Technology, Cambridge, Massachusetts 02139, USA*
[3]*Department of Nuclear, Plasma, and Radiological Engineering, University of Illinois at Urbana-Champaign, Urbana, Illinois 61801, USA*
[4]*National Synchrotron Radiation Research Center, Hsinchu 300, Taiwan*

(Received 22 April 2013; accepted 17 July 2013; published online 12 August 2013)

A synchrotron X-ray diffraction method was used to measure the average density of water (H_2O) confined in mesoporous silica materials MCM-41-S-15 and MCM-41-S-24. The average density versus temperature at atmospheric pressure of deeply cooled water is obtained by monitoring the intensity change of the MCM-41-S Bragg peaks, which is directly related to the scattering length density contrast between the silica matrix and the confined water. Within MCM-41-S-15, the pore size is small enough to prevent the crystallization at least down to 130 K. Besides the well-known density maximum at 277 K, a density minimum is observed at 200 K for the confined water, below which a regular thermal expansion behavior is restored. Within MCM-41-S-24 of larger pore size, water freezes at 220.5 K. The average water/ice density measurement in MCM-41-S-24 validated the diffraction method. The anomalous thermal expansion coefficient (α_p) is calculated. The temperature at which the α_p reaches maximum is found to be pore size independent, but the peak height of the α_p maximum is linearly dependent on the pore size. The obtained data are critical to verify available theoretical and computational models of water. © *2013 AIP Publishing LLC*. [http://dx.doi.org/10.1063/1.4817186]

I. INTRODUCTION

Water is the most important liquid in both daily life and many branches of science.[1] A number of water's fascinating anomalies[2] become more pronounced at supercooled temperatures.[3,4] In fact, several second order thermodynamic response functions, such as the compressibility and the heat capacity,[5,6] have been found to increase monotonically as the temperature decreases, implying very large fluctuations at low temperatures. The existence of a low-to-high density liquid-liquid phase transition (LLPT)[7–10] in the low temperature regime has been proposed (and debated[11,12]) to coherently explain these anomalies.[8,13–20] However, on the experimental side, the situation is more ambiguous because the homogeneous ice nucleation makes liquid water at temperatures lower than 235 K experimentally inaccessible. On the other hand, water under strong confinement can be cooled down below the bulk homogenous nucleation point without freezing into crystalline ices due to the finite size and surface effect. Confined water is a worth-studying system[7,21–33] that is ubiquitous in many physicochemical processes.

Recently, we have approached this "no-man's land[8]" of temperature region by examining water confined in very small pores (of diameter less than 1.6 nm). The confined water does not freeze down to lower than 130 K. Quasi-Elastic Neutron Scattering (QENS) studies have been performed to study H_2O's diffusional dynamics[13,22,23,26,34–36] and Small Angle Neutron Scattering (SANS) have been performed to understand D_2O down to deeply cooled region.[37–41] In 2007, we discovered the existence of a density minimum at 210 K for confined D_2O by SANS.[37] More recently, we have measured the densities of confined D_2O at elevated pressures (1–2900 bar) using a Triple-Axis spectrometer at the elastic scattering mode. An interesting hysteresis of density versus temperature developed at high pressures (above 1000 bar).[38] This phenomenon was interpreted as an evidence of crossing the remnant first order transition line between a low-density liquid (LDL) and a high-density liquid (HDL) state of heavy water in the finite system. Experimental findings in the deeply cooled confined water and their implications for the LLPT hypothesis of bulk water have recently been reviewed by Bertrand *et al.*[42]

Ordinary water (H_2O) is more important than the heavy water D_2O in science and in many applications. Therefore, despite a similar trend can be expected, the density of H_2O at deeply cooled temperatures in confined space is worthy to be measured separately. In a previous study using vibrational spectra, the density of water as a function of temperature was estimated by fitting the vibrational spectra into four components and assuming constant densities for each component.[30,31] Therefore, it is an indirect method. It is rather uncertain how the assumptions in the data analysis would affect the density result. On the other hand, the SANS method used to determine the average density of heavy water D_2O

a)Author to whom correspondence should be addressed. Electronic mail: cymou@ntu.edu.tw

 © 2013 AIP Publishing LLC

This article is copyrighted as indicated in the abstract. Reuse of AIP content is subject to the terms at: http://scitation.aip.org/termsconditions. Downloaded to IP: 140.110.200.123 On: Mon, 25 Nov 2013 06:41:17

suffers a limitation for ordinary water because of its relative small neutron coherent scattering length density.[40] Thus up to the present, no reliable density data for H_2O down to deeply cooled region exists.[43]

Here, we used synchrotron X-ray diffraction peaks of water confined in mesoporous silica to determine the average density of H_2O, taking advantage of the suitable scattering length density of water with respect to X-ray. Besides, the high flux and high signal-to-noise ratio of X-ray diffraction can provide more reliable and higher Q-resolution data. A direct measurement of the average density of deeply cooled H_2O confined in MCM-41-S was performed with synchrotron X-ray diffraction, on both heating and cooling scans between 300 K and 150 K. This paper should be considered not only a validation of the former neutron results on D_2O but also an independent study of H_2O. The synchrotron method presented is an improved diffraction technique for measuring the average density of confined liquid as well.

II. EXPERIMENTAL

A. Materials

The mesoporous silica MCM-41-S-15 powder sample is made by calcining micellar templated silica matrices, which consist of grains of micrometer size. In each grain, parallel cylindrical pores are arranged in a 2D hexagonal lattice with an inter-plane distance $d = 29$ Å. It is synthesized by reacting pre-formed β-zeolite seeds (composed of tetraethylammonium hydroxide (TEAOH, Acros), sodium hydroxide (NaOH), and fumed silica (Sigma)) with decyltrimethylammonium bromide solution (C_{10}TAB, Acros). The mixture is transferred into an autoclave at 120 °C for 2 days. After cooling to room temperature, the mixture was adjust to pH = 10, and sealed in an autoclave at 100 °C for 2 days. Solid sample is collected by filtration, washed by water and ethanol, dried at 60 °C in air overnight, and then calcined at 540 °C for 8 h. The molar ratios of there actants are SiO_2:NaOH:TEAOH:C_{10}TAB:H_2O = 1:0.075:0.285:0.204:226.46. The use of β-zeolite seeds as a silica source makes the silica pore walls semi-crystalline and resistant to hydrolysis decay.[44]

MCM-41-S-24, and other MCM family samples used in the Differential Scanning Calorimetry (DSC) measurements are synthesized by similar procedures, only using different carbon chain length surfactants or hydrothermal treatments. The difference between the two series of MCM-41 is undergoing the second hydrothermal process or not. MCM-41-S-15 and MCM-41-S-24 used in this study, together with other MCM-41-S samples labeled in red dots are treated with the second hydrothermal (two of MCM-48-S samples are also treated with the second hydrothermal), thus have even stronger structure and better hydrolysis resistant. More details can be found in Ref. 45.

A 10 wt.% of gold powder (1.5–3 μm, Acros) was mixed with the MCM-41-S-15 and MCM-41-S-24 powder. The gold powder is used as an internal reference for the X-ray intensity. The sample was then hydrated by exposing it to undersaturated water vapor in a closed container until a full hydration level was achieved.

B. Instruments

The X-ray diffraction experiment was performed at the beamline 17A1 of Taiwan Light Source (TLS) at the National Synchrotron Radiation Research Center (NSRRC) in Taiwan. The incident X-ray energy is fixed at 9.297 KeV (1.3336 Å wavelength).

The hydrated MCM-41-S-15 sample was tightly packed and sealed in a 1.0 mm glass capillary and then aligned in the X-ray beam. The sample environment was controlled by a low temperature nitrogen gas cryo-jet system (Oxford instruments). A Mar 3450 on-line IP scanner was used as a detector. The experimental setup was transmittance mode, sample and X-ray beam were located at the center of imagine plate. Every temperature point was exposed three times (120 sec each time) and averaged to assure the data quality.

The temperature at the sample position was calibrated by an external thermal couple before use. Temperature is ramped to equilibrate at every 5 K interval with a temperature accuracy of ±0.1 K. When a temperature set-point was reached, the sample was equilibrated for 5 min before the X-ray exposure. The capillary was continuously rotated at 2 Hz to avoid local heating or inhomogeneous exposure.

The hydrated MCM-41-S-24 sample was tightly packed and sealed in an alumina pan. Holes were punched in both sides of the pan and sealed with Kapton films for X-ray passage. A liquid nitrogen control system (LNCS) was used in this set of experiments. The temperature was continuously ramped at a rate of 0.67 K/min in both cooling and heating scans. This slow ramping rate guarantees a uniform temperature distribution in the sample. A Mar 3450 on-line IP scanner was also used as the detector, but it was operated in continuous mode. Each frame was exposed for 72 sec, and read out for 108 sec. This setup can obtain 2 K/frame.

III. RESULTS AND DISCUSSION

First, we start with the characterization of the MCM-41-S materials. The pore diameter of MCM-41-S-15 and MCM-41-S-24 are estimated to be 15 Å and 24 Å, respectively (Figure 1) with the Barret-Joyner-Halenda (BJH) method,[46] which is based on the Kelvin equation.[47] Refinements allow the reduction of the physical pore size by the thickness of the adsorbed film existing at the critical condensation pressure. Further refinements adjust the film thickness for the curvature of the pore wall. Here in our case, the Hasley[48] thickness equation and Faas correction were applied to our isotherms and gave the pore size distribution (PSD). The maximum point of PSD was chosen as the nominal pore size of our samples. It is well known that the pore size is underestimated by this thermodynamics-based BJH method, especially for such a small pore sizes, because there are one or two layers of nitrogen that are adsorbed tightly on the surface of silica pore (giving Brunauer-Emmett-Teller (BET) surface area) before the capillary condensation. The reported BJH pore diameter does not include this tightly bond layer. If one wants to estimate the bare diameter (silica-wall-to-silica-wall), it may be closer to 20 Å for MCM-41-S-15. To the best of our knowledge, there is no method that can provide a more precise estimate of the pore size at this scale. In this paper, the 15 Å and

This article is copyrighted as indicated in the abstract. Reuse of AIP content is subject to the terms at: http://scitation.aip.org/termsconditions. Downloaded to IP: 140.110.200.123 On: Mon, 25 Nov 2013 06:41:17

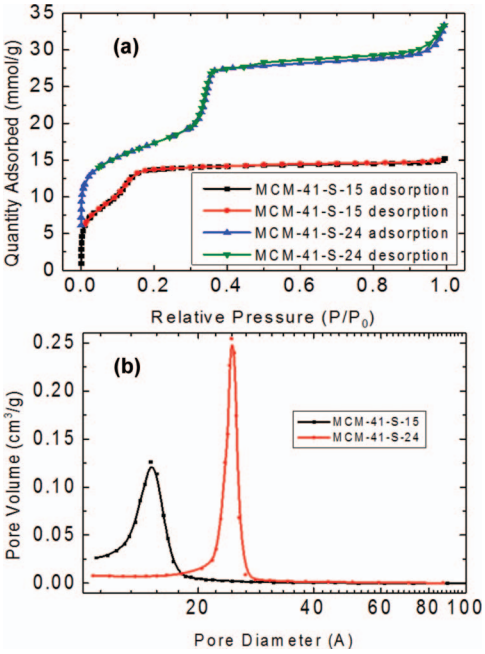

FIG. 1. (a) Nitrogen adsorption/desorption isotherms at 77 K. The isotherms of MCM-41-S-24 are shifted by 5 mmol/g for clearness. (b) BJH adsorption dV/dD pore size distributions calculated by BJH method with default parameters of Halsey thickness curve and Faas correction. One should note that the pore sizes may be underestimated by this method. The idea of a nominal BJH pore size is only for convenience to compare with other similar materials.

24 Å are nominal diameters. We have used the BJH nominal diameter as part of the sample name and the fitting parameter below.

The well-ordered pore structure of MCM-41-S-15 can be clearly seen in the high resolution transmission micrograph presented in Figure 2(a). In Figure 2(b), DSC results show that there is neither freezing of bulk external water nor freezing of confined water in the non-freezing sample (MCM-41-S-15) down to 130 K. The glass transition temperature of bulk water was reported to be either 136 K or 165 K.[49] It is tempting to assume that our confined water remains liquid state down to at least 200 K, below which it may evolve into certain amorphous form. In the same figure, we make comparison with the DSC data of a deliberately overloaded sample of MCM-41-S-24 of 24 Å pore diameter. One can see a clear endothermic melting peak at 224 K due to the water inside the pores and a peak near 268 K due to the excess water outside the pore opens. Careful loading to avoid external water is achieved by taking a water vapor adsorption isotherm, which is shown in Figure 2(c). The water condensates at the relative pressure (P/P_0) of about 0.35–0.4 into the nanopores. There is no further condensation in the range of $0.5 < P/P_0 < 0.7$. So we can make sure that water is loaded inside the nanopores by controlling the relative pressure of water vapor in the range of 0.5–0.7. This helps us to realize the water vapor pressure necessary for capillary condensation, but which is low enough to avoid condensation on the external surface. For the sample of Figure 2(c), the capillary condensation water should be 0.41 g/g (water mass/dry silica mass) at the loading partial pressure of water based on adsorption isotherm shown. According to thermogravity analysis (TGA), the hydration level by weight is 0.45 g/g. The two values are close confirming that all the mesopores are filled, while there is negligible external water (Figure 2(c)).

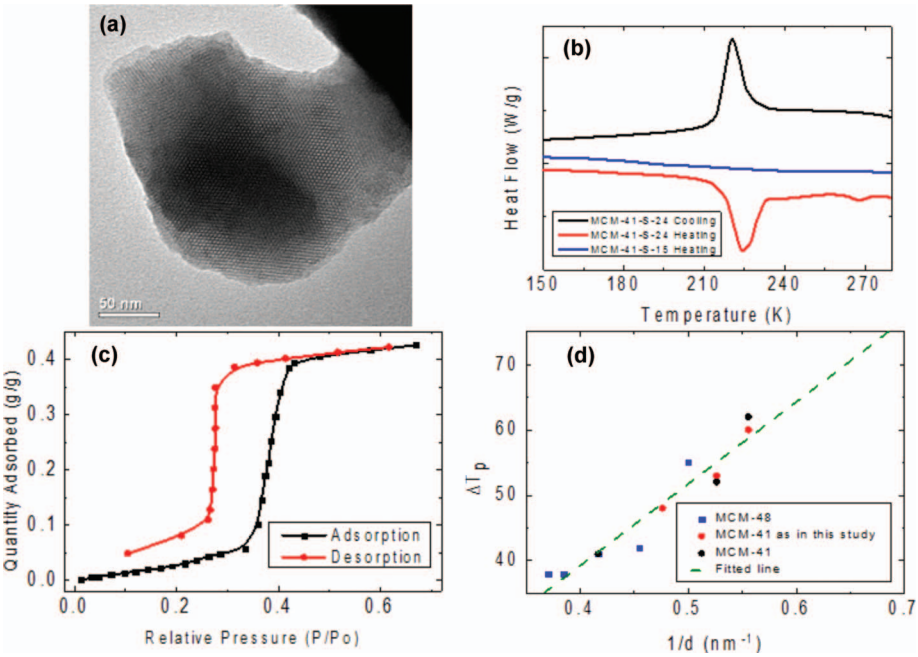

FIG. 2. (a) High resolution transmission microscopy graph of MCM-41-S-15. The 2D hexagonal pore structure can be clearly seen. (b) DSC scans of water confined in MCM-41-S mesoporous silica materials for two pore sizes. The last two digits of the labels denote the nominal pore size in Å calculated by BJH method. (c) Water vapor adsorption and desorption isotherms at 298 K. (d) The Gibbs-Thomson equation plot. The dots are data from MCM-41. Black and red dots stand for two different procedures of MCM-41. MCM-41-S-15 used in this study is synthesized by the same procedure as the red dots. Blue squares are data from MCM-48. All materials' pore sizes are characterized by BJH method. Despite different kinds of mesoporous silica, all the data follow a linear relation. The crystallization of confined water is bypassed within the materials of pore size smaller than about 1.6 nm.

This article is copyrighted as indicated in the abstract. Reuse of AIP content is subject to the terms at: http://scitation.aip.org/termsconditions. Downloaded to IP: 140.110.200.123 On: Mon, 25 Nov 2013 06:41:17

In the MCM family of mesoporous silica materials, it is easy to control the pore size and structure geometry by choosing surfactants of different carbon chain lengths and hydrothermal conditions. For instance, the 2D hexagonal phase of MCM-41 (*P*6 mm symmetry), lamellar phase of MCM-50, and 3D cubic phase of MCM-48 (*I*a3d symmetry) are the three most studied structures.[50] We have synthesized MCM-41 and MCM-48 of many different pore sizes, and then measured their BJH diameters and melting point T_p by DSC. Figure 2(d) plots the melting point depression ΔT_p as a function of inverse pore diameter (BJH) of several series of MCM materials. In spite of the structure geometry difference between MCM-41 and MCM-48, and different procedures of fabricating the two series of MCM-41, all the data follow the Gibbs-Thomson equation. Even though it has been pointed out in the literature that the Gibbs-Thomson equation does not hold for very small pores,[51,52] our data show that the thermodynamic relation is still, within the measurement accuracy, valid in our pore size range of interest.[27,53,54] The fitting result also suggests that water confined in these materials is rather homogeneous in the pores, or at least, no obviously distribution change at low temperatures was observed. As a matter of fact, the silanol surface would affect the hydrogen bond network between water molecules from the interface to the center in the pores, however it only results in a slightly higher density layer near the surface.[7,25,29,55–59] In addition, no experimental evidence for the existence of microstructures on silica walls of MCM materials were reported to allow the penetration of water and alter the water density distribution. From the fitted slope, one can obtain the surface free energy of ice-water interface as $\gamma_{SL} = 38.3$ mJ/m^2. The value is close to the ice/water surface free energy in bulk water (33 mJ/m^2)[60] considering the substantial uncertainty in the measurements.

A typical diffraction pattern of hydrated MCM-41-S-15 is shown in Figure 3(a). One can see the three Bragg peaks of the MCM-41-S-15 material loaded with water ((100), (110), (200) at $2\theta = 1°$–$6°$ or Q = 0.09–0.5 Å^{-1}) and the gold diffraction peaks at high angle. Because the structure remains the same in all measurements and the pores are fully filled with water, the scattering intensity (I) is related only to the contrast between the silica matrix and the average water density inside the pores. More precisely, it is proportional to $(\rho_{MCM}-\rho_{water})^2$. Since the MCM-41-S-15 is rigid and the wall silica density ρ_{MCM} does not change in this temperature range, the relative ρ_{water} can be deduced by measuring the diffraction intensity change. (ρ_{MCM} and ρ_{water} are the scattering length density (SLD) of MCM-41-S-15 and water, respectively, and are proportional to their mass density.) In the low Q limit, our small angle scattering method probes only the large-scale spatial fluctuations. Therefore, water as well as the confinement can be considered as continuum. We do not detect any molecular structure factor peaks, which are located at much higher Q values than the water cylinder-cylinder Bragg peaks. For the same reason, the surface layer water structure caused by interactions with the silica surfaces is not observable in the Q range, either.

Dry MCM-41-S-15 was measured in the same manner. The normalized diffraction intensity of the dry sample is much higher and remains constant through 300–150 K

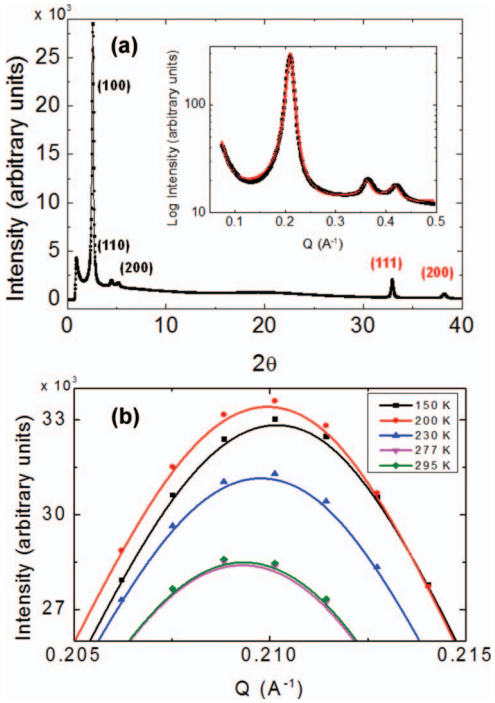

FIG. 3. (a) The diffraction pattern of H_2O confined in MCM-41-S-15 with 10 wt.% of gold particles as internal standard at 300 K. Black notations at low angles denote the Bragg peaks from the ordered porous structure of MCM-41-S-15, and the red notations at high angles are the Bragg peaks from gold lattice. The inset shows the low angle diffraction used in our analysis. The black squares are normalized data points, and the red line is the fitted curve. (b) Enlarged (100) peaks of hydrated MCM-41-S-15 at different temperatures. After normalization by the intensity of gold diffraction, the diffraction intensity change can be related to the contrast variation between the silica matrix and the confined water.

(Figure 4(a)). Neither structure nor intensity change was observed for the silica matrix. To deal with the intensity fluctuation of the incoming X-ray beam, the diffraction intensities of MCM-41-S-15 were normalized by the diffraction intensities of gold (111) (Figure 4(b)) in each measurement. We note here that any possible external water would not affect our result since only the water inside the pores contributes to the intensity of the Bragg peaks.

The tops of the (100) peaks at five different temperatures are shown in Figure 3(b). From 295 K to 277 K, the small intensity drop shows a contrast decrease and directly reflects water's increasing density from 300 K to 277 K. From 277 K to 200 K, as the temperature was decreased, the intensity rise showed a contrast increased and the average water density thus decreased. When the sample was deeply cooled below 200 K, the intensity drop showed that the water density increased slightly again, and exhibited a density minimum in-between. This initial examination confirmed that the density maximum and minimum behaviors are real physical phenomena and independent to our fitting model. The peak position seems to show a slight change (<0.001 Å^{-1}) with temperatures. However, it is hard to draw any concrete conclusions about this change considering the instrumental resolution.

The diffraction intensity I(Q) can be described by the theory of small angle scattering as

$$I(Q) = nV_P^2(\Delta\rho_{SLD})^2 P(Q)S(Q), \quad (1)$$

This article is copyrighted as indicated in the abstract. Reuse of AIP content is subject to the terms at: http://scitation.aip.org/termsconditions. Downloaded to IP: 140.110.200.123 On: Mon, 25 Nov 2013 06:41:17

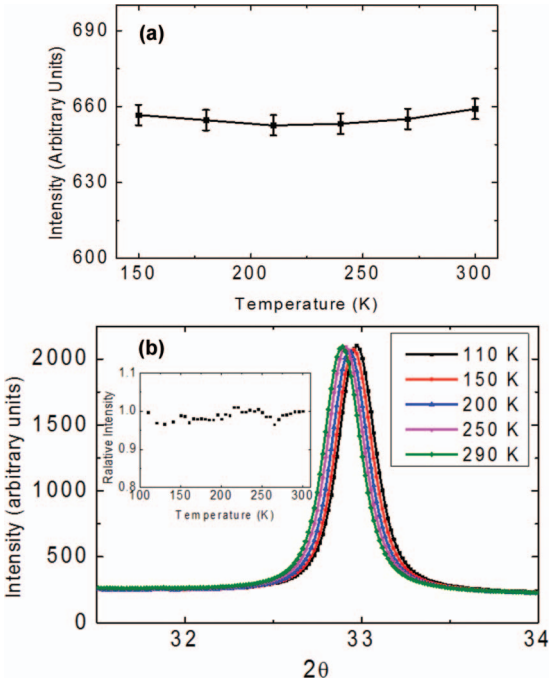

FIG. 4. (a) The normalized diffraction peak intensities of dry MCM-41-S-15 at different temperatures. Compared to the intensity change of 15% seen in hydrated MCM-41-S-15, the intensity variation of dry MCM-41-S-15 is within 1%. This demonstrates that the density change of MCM-41-S-15 over the experimental temperature range is negligible and justifies our assumption that the SLD of MCM-41-S-15 is constant. The trend of diffraction intensity only varied with the water density change. (b) Diffraction peaks of gold (111) at selected temperatures. The peak shape remains the same. Only the peak position slightly shifts toward higher angle as temperature decreases because of the thermal contraction of gold lattice. (Inset) Diffraction intensities of gold (111) at all temperature range. The intensities are normalized to the intensity of 300 K. The intensity fluctuation is within about 5%, which solely results from the fluctuation of synchrotron beam flux.

where n is the number of scattering units (water cylinders) per unit volume, V_p is the volume of the scattering unit, $\Delta\rho_{SLD} = \rho_{MCM} - \rho_{water}$ is the difference of SLD between the scattering unit water and the silica matrix, P(Q) is the normalized particle structure factor (or form factor) of the scattering unit, and S(Q) is the inter-cylinder structure factor of a 2D hexagonal lattice. The SLD of water and MCM-41-S-15 can be calculated from their mass density ρ^{m} by the factor $\alpha = (b_e N_A \sum n_i Z_i)/M$, where b_e is the coherent scattering length of electron, which has a value of 2.818×10^{-13} cm, N_A is the Avogadro's number, $\sum n_i Z_i$ is the total number of electrons in the scattering unit, and M is the molecular weight of the scattering unit. The SLD of MCM-41-S-15 was determined by assuming its chemical formula was SiO_2. The mass density of it was measured by helium gas pycnometer to give a value of 2.20 g/cm^3. The thermal expansion coefficient of the silica matrix is about three orders smaller than that of water. Therefore, MCM-41-S-15 is regarded as rigid in our data analysis, i.e., its SLD is temperature independent. Throughout the experimental temperature range, the position and the width of the Bragg peaks remained the same, proving that any structural changes of MCM-41-S-15 could be neglected. Based on these considerations, one can conclude that ρ_{water} is the only temperature dependent factor in the expression of I(Q). Hence, we can obtain the average mass density of H_2O by measuring the X-ray diffraction intensities as a function of temperature. The correction to this average density approach coming from the more realistic layering structure of water inside the pores has been carefully examined.[41] It has been argued that the correction is not more than 10% and is therefore negligible.

The form factor P(Q) of a long ($QL > 2\pi$) cylinder is given by

$$P(Q) = \frac{\pi}{QL}\left(\frac{2J_1(QR)}{QR}\right)^2, \tag{2}$$

where L and R represent the length and the radius of the cylinder, respectively, and J_1 is the first-order Bessel function of the first kind. The structure factor S(Q) can be approximated by a Lorentzian function. The Q positions of the (100), (110), and (200) peaks of a 2D hexagonal symmetry have the relation of $1{:}\sqrt{3}{:}2$. A temperature independent power law background originating from the fractal packing of the grains and air scattering, together with a very small Q-independent background were also added. Therefore, the measured X-ray scattering intensity can be expressed as

$$\begin{aligned} I(Q) = {} & nV_P^2\left(\alpha\rho^m_{water} - \rho^{SLD}_{MCM}\right)^2 \frac{\pi}{QL}\left(\frac{2J_1(QR)}{QR}\right)^2 \\ & \times\left[\left(\frac{\frac{1}{2}\Gamma_1}{\left(Q-\frac{2\pi}{d}\right)^2+\left(\frac{1}{2}\Gamma_1\right)^2}\right)\right. \\ & + f_2\left(\frac{\frac{1}{2}\Gamma_2}{\left(Q-\frac{\sqrt{3}\times 2\pi}{d}\right)^2+\left(\frac{1}{2}\Gamma_2\right)^2}\right) \\ & \left.+ f_3\left(\frac{\frac{1}{2}\Gamma_3}{\left(Q-\frac{2\times 2\pi}{d}\right)^2+\left(\frac{1}{2}\Gamma_3\right)^2}\right)\right] + B\times Q^{-\beta} + C, \end{aligned} \tag{3}$$

where Γ_1, Γ_2, Γ_3 are the FWHM of (100), (111), (200) peaks, respectively, f_2, f_3 are the intensity factors of (110) and (200) peaks to (100) peak, respectively, C is the Q-independent background. The approximation of the diffraction pattern by this function is pseudo-empirical. The broadening of a diffraction peak comes from many factors, such as the imperfection of the lattice and the grain sizes. The form factor is also simplified and does not include a smear term to describe the pore size distribution. We have used these simplified functions to reduce the number of fitting parameters. One should notice that since the function is pseudo-empirical, the fitted values of radius, FWHM, and intensity factors should not be considered as precise values. In fact, the radius of this function was fixed at 7.5 Å, which is the value obtained from the nitrogen sorption experiment, to further simplify the fitting. We confirmed that this assumption was not over-parametrized by fixing the radius at values between 6 and 12 Å and got similar results. The choice of the precise form for the peak formula and the simplified form factor model will not affect the extraction of the average density of water, which merely depends on the diffraction intensity.

By fitting the X-ray diffraction intensities globally (to include all three Bragg peaks) with the above-described model

This article is copyrighted as indicated in the abstract. Reuse of AIP content is subject to the terms at: http://scitation.aip.org/termsconditions. Downloaded to IP: 140.110.200.123 On: Mon, 25 Nov 2013 06:41:17

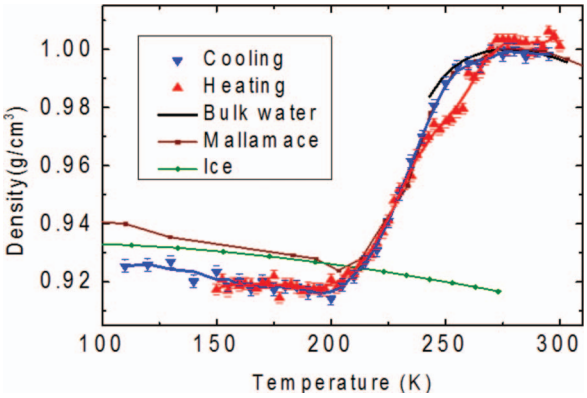

FIG. 5. The average water density derived from the diffraction intensities compared with bulk water density above T_H, ice I_h density, and Mallamace's calculation from vibrational spectra.[30] The density maximum at 277 K and minimum at 200 K can be seen. The density minimum is found to be 0.914 $\pm$ 0.002 g/cm^3.

at each temperature, the temperature independent background can be subtracted, and the temperature dependent intensities I(T) can be extracted. When this is done, all the other temperature independent parts can be regarded as constants and that can be determined by normalizing the density at 277 K to the bulk density of H_2O.

In Figure 5, the extracted average density of confined H_2O is shown. We first cooled down the sample to 150 K, at which we started to record the heating data until 300 K; then the sample was cooled again and the cooling data were recorded. The difference between 240 K and 260 K is not significant compared to the hysteresis loop reported at high pressures.[38] Other than that, the two sets of data are highly consistent with each other showing that our experimental results are quite stable and robust. In Figure 5, we have also included the bulk water and ice I_h density from CRC handbook,[61] Mallamace's estimation from measurements of vibrational spectra[30] of MCM-41-S-15 confined water, and data from our measurements. One can find that they follow similar trend. Although Mallamace's data and our data deviate slightly in deeply cooled region, these two methods both reveal comparable trends and a similar density minimum. Compared to the density of D_2O from SANS measurements,[37] the densities also show strongly parallel behavior. Compared to confined D_2O, the density maximum temperature down shifts $\sim$7 K (284 K in D_2O, and 277 K in H_2O), and the density minimum temperature down shifts 10 K (210 K in D_2O, and 200 K in H_2O). The density change between maximum and minimum is a bit bigger, 8.6% for H_2O versus 5.8% for D_2O. Below the temperature of the density maximum, an open four-coordinated network of hydrogen bonds increasingly develops and occupies more volume, which overwhelms the normal tendency of contraction when cooled. However, this anomaly must reach an end when the hydrogen bonds network fully expands, then the contraction dominates again. The H_2O density of our measurements reveals a density minimum and suggests that the structure of water below the temperature minimum is approaching an open random tetrahedral network of hydrogen bonds.

Now it is relevant to discuss the effects of confinement and the hydrophilic silica surface on the density minimum of water. Indeed, the nanopores of MCM-41-S play a big role in stabilizing water at such a low temperature. Bulk water crystallizes because it lacks a surface energy penalty. However, such a difficulty could be solved by short-time molecular dynamics (MD) simulations,[62–67] so that predictions of the properties of bulk water could be made. It is interesting to find out that the density minimum originally predicted for bulk water also exists in confined water. Therefore, it is tempting to associate our experimental observations to the intrinsic properties of water. The density drop for H_2O at low temperature is so large that the density of water below 215 K is even less than that of ice I_h. It is not clear whether this is due to a more open structure or due to the way we normalize the absolute density of confined water to the bulk at 277 K. The normalization may be a source of systematic error in our analysis. On the other hand, there is no theoretical argument that density of water should be higher than that of ice. In fact, most solids have higher density than their liquid phases. Even ice has several polymorphism forms denser than liquid water. There might be a chance that deeply cooled water under confinement reverts to "normal" liquid again, just like it does under high-pressure conditions. Anyway, the absolute density is beyond the scope of the present work and requires further investigations. We emphasize that the thermal expansion coefficient calculated later in this paper is not affected by this scaling or the density data lower than 215 K.

The idea of using small angle scattering to measure the average density of confined water has been criticized. It was argued that the density of water inside the pores may be very inhomogeneously distributed or a huge amount of water would penetrate into the silica wall, so that the scattering intensity variation obtained by the small angle scattering method cannot be regarded as a measurement of the average density of water, but only the distribution inside the pores changed.[68–70]

To address these comments, a comparison experiment was performed on water confined in a larger pore size system, MCM-41-S-24, which has the nominal BJH pore size of 24 Å. The DSC scans of water confined in MCM-41-S-24 (Figure 2(b)) show that the freezing of water does happen at 220.5 K. Figure 6 demonstrates the difference between H_2O confined in MCM-41-S-15 and MCM-41-S-24 by showing their X-ray diffraction patterns focused on the 2θ angle range of oxygen-oxygen arrangement of confined water. At 300 K, water confined in both materials show only a very broad peak, which can be assigned to liquid water. At 170 K, the liquid water peak does not change much in MCM-41-S-15 (only three very small peaks come from minor overfilled ice I_h), which implies that the confined water remains in liquid state at low temperature. On the other hand, a broad ice I_c peak appears in MCM-41-S-24 sample. By Scherrer's equation, the crystal size is found about the same as the pore size as 24.7 Å, suggesting the ice formed inside the pores of MCM-41-S-24.

As described previously, the average density of water/ice as a function of temperature can be obtained for the MCM-41-S-24 sample (Figure 7). Here, the observed trend is similar to

This article is copyrighted as indicated in the abstract. Reuse of AIP content is subject to the terms at: http://scitation.aip.org/termsconditions. Downloaded to IP: 140.110.200.123 On: Mon, 25 Nov 2013 06:41:17

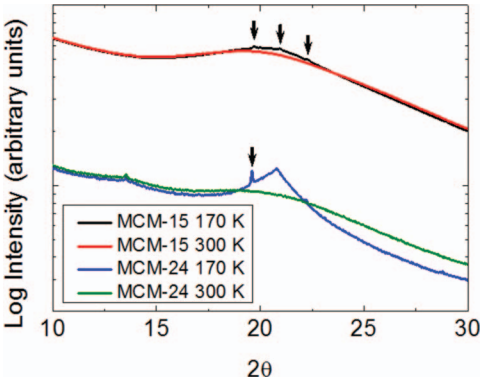

FIG. 6. The XRD patterns of H2O confined in MCM-41-S-15 and MCM-41-S-24 focused on the 2θ angle range of oxygen-oxygen arrangement at different temperatures. The small sharp peaks marked by arrows are assigned to be ice I_h with large crystal size. A broad ice I_c peak with crystal size of 24.7 Å centered at 20.7° can be seen in MCM-41-S-24 sample only, which suggests H_2O freezing inside the pores of 24 Å, while remaining liquid inside the pores of 15 Å.

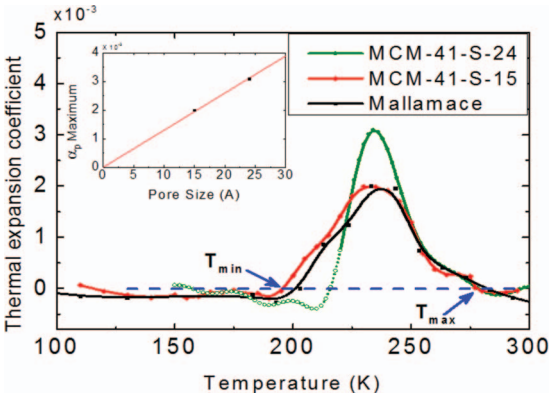

FIG. 8. Thermal expansion coefficient of H_2O confined in MCM-41-S-15 and MCM-41-S-24 compared with Mallamace's calculation. In the case of MCM-41-S-24, filled symbols and solid line represent liquid water, while empty symbols and dotted line represent ice. The blue dashed line is zero of thermal expansion coefficient. The two blue arrows point out the temperatures of the density maximum and minimum, which are denoted as T_{max} and T_{min}, respectively. The inset shows the maximum of α_p are proportional to the pore sizes with zero intercept.

the MCM-41-S-15 case. Probably due to a more stable temperature control system used in the measurement, the densities of cooling and heating scans are almost identical to each other. Even the small difference noted around 250 K in the MCM-41-S-15 case is not seen. The average density above T_H is comparable to the density of bulk water, and the density maximum is also clearly seen. More importantly, one can find the average density below the freezing temperature is very close to the density of bulk ice density. If the density distribution inside the pores fluctuated with temperature, it would be impossible to obtain the average density same as bulk water at high temperature and also same as bulk ice at low temperature. The data suggest that the water distribution inside nanopores can be considered rather homogeneous and highly bulk-like in a well-prepared and fully hydrated sample.

Ideally, the density curves should be scaled by the absolute density of confined water at room temperature. Unfortunately, the absolute density of confined water is not known exactly. According to the weight of hydration water and the pore volume measured by nitrogen adsorption, the density of confined water is roughly in the range of 0.9 g/cm^3, lower than the bulk. This is consistent with work reported in the literature showing that the hydrophilicly confined water has a slightly lower density than the bulk. Our SAXS method determines the relative density up to one scaling factor. Keeping this in mind, we chose to scale our determined relative density of the confined water to the density of bulk water at room temperature so that it is easier to compare with other density data. By no means, they stand for the absolute density of the confined water. However, when calculating the thermal expansion coefficient, this scaling factor is canceled out. Figure 8 shows the thermal expansion coefficients calculated by $\alpha_p = -\frac{1}{\rho}\frac{d\rho}{dT}$. The points at which thermal expansion coefficient crosses zero represent the density extrema. The deduced thermal expansion coefficient is quite close to the results reported in Mallamace's work.[30]

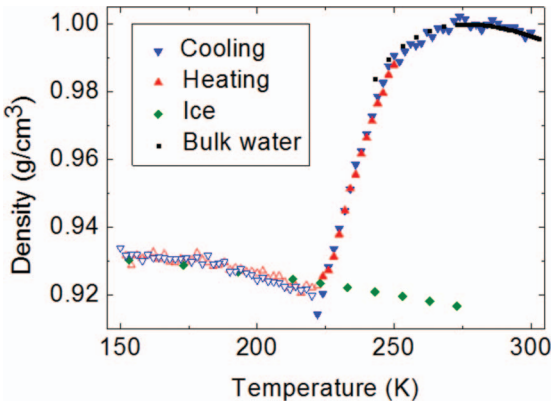

FIG. 7. The average H_2O density confined in MCM-41-S-24 compared with water and ice I_h density in their bulk form. Both in the heating and cooling scans, filled symbols represent liquid water, and empty symbols represent solid ice.

The inflection point in the density profile implies that α_p has a sharp peak (at 230 K) between the two temperatures of the density extrema (Figure 8). Coincidentally, previous studies of the same confined water have shown that the transport coefficients show a fragile-to-strong dynamic crossover phenomenon at 225 ± 5 K by QENS[23] and NMR,[71] and the Stokes-Einstein relation breaks down at the same temperature.[72] Now with the new expansion coefficient data, it is striking to find out that the dynamic and thermodynamic properties of confined water seem to change behaviors at the same temperature around 230 K. This feature can be explained by the hypothesis of a liquid-liquid critical point (LLCP) at high pressures. In the LLCP picture, supercooled water has two phases characterized with two different densities, which are separated by a first-order transition at high pressures and low temperatures. While at ambient pressure, the density fluctuations along the extension of the phase transition line, although not divergent, show a maximum in the one-phase region, known as the "Widom line."[73] The single thermodynamic and dynamic crossover temperature at around 230 K, although cannot prove, agrees with this picture.

This article is copyrighted as indicated in the abstract. Reuse of AIP content is subject to the terms at: http://scitation.aip.org/termsconditions. Downloaded to IP: 140.110.200.123 On: Mon, 25 Nov 2013 06:41:17

For the MCM-41-S-24 sample, if we disregard the data below freezing point in MCM-41-S-24 sample at 220.5 K, it still reveals a sharp peak at around 230 K, well above the freezing happens. So it is a liquid state phenomenon. The inflection points of the two samples with different pore sizes show up at almost the same temperature, suggesting that the average density we determined and the thermal expansion coefficient we calculated as a function of temperature are intrinsic properties of the confined water. Furthermore, a simple plot of the peak height of the expansion coefficient versus the nominal pore size of the silica material shows a nice scaling behavior that goes through the zero point. Near a regular critical point, the thermodynamic response functions diverge together with the correlation length following power-laws with the corresponding critical exponents. In our experiments, if we assume the correlation length is limited by the pore size, it seems that the maximum expansion coefficient scales nicely with the nominal pore size (inset of Figure 8). Although the measurement was taken at ambient pressure (may be subjected to the Laplace pressure to some extent but we do not consider it in this paper), far away from the hypothesized second critical point of water, it is tempting to associate the peaking of the expansion coefficient to the hypothesized Widom line. Clearly, more studies of the scaling behavior are needed to make concrete conclusions.

IV. CONCLUSION

The mesopores of the well-ordered silica matrix MCM-41-S-15 were used to confine water and thereby suppress the ice formation and make the "no man's land" water accessible for experimental study. We report a careful characterization of the MCM-41-S materials loaded with water to show that the confined water does not freeze inside the pores and there is only negligible amount of external water. Synchrotron X-ray diffraction measurements were analyzed to determine the average density of the confined water in deeply cooled region were reported. Both a density maximum at 277 K and a density minimum at 200 $\pm$ 2.5 K were obtained. The properties of water in a larger pore size sample, MCM-41-S-24, in which the confined water freezes below 220.5 K, were also observed and used to validate our methodology. The thermal expansion coefficient α_p derived from the density curves of difference pore sizes show maxima around 230 K, which are pore size independent. However, the values of the α_p maxima follow linear dependence on the pore size. The thermodynamic and dynamic implications of the maxima in thermal expansion coefficient were discussed.

ACKNOWLEDGMENTS

The authors appreciate the beam time from National Synchrotron Radiation Research Center in Taiwan, and great efforts of the 17A1 beamline manager, Dr. Ching-Yuan Cheng and the 23A1 beamline assistant, Mr. Wen-Bin Su, for the setup of experiments. Special thanks to Dr. C. E. Bertrand for proof reading this paper. The research at National Taiwan University by Taiwan National Science Council Grant No. NSC99-2120-M-002-008 and the research at Massachusetts Institute of Technology is supported by Department of Energy Grant No. DE-FG02-90ER45429.

[1] P. Ball, *Life's Matrix: A Biography of Water* (University of California Press, 2001).
[2] P. Ball, Nature (London) **452**, 291 (2008).
[3] L. M. Xu, F. Mallamace, Z. Y. Yan, F. W. Starr, S. V. Buldyrev, and H. E. Stanley, Nat. Phys. **5**, 565 (2009).
[4] P. G. Debenedetti, J. Phys.: Condens. Matter **15**, R1669 (2003).
[5] H. E. Stanley, P. Kumar, L. Xu, Z. Yan, M. G. Mazza, S. V. Buldyrev, S. H. Chen, and F. Mallamace, Physica A **386**, 729 (2007).
[6] A. Nagoe, Y. Kanke, M. Oguni, and S. Namba, J. Phys. Chem. B **114**, 13940 (2010).
[7] P. Gallo, M. Rovere, and S. H. Chen, J. Phys. Chem. Lett. **1**, 729 (2010).
[8] O. Mishima and H. E. Stanley, Nature (London) **396**, 329 (1998).
[9] K. Stokely, M. G. Mazza, H. E. Stanley, and G. Franzese, Proc. Natl. Acad. Sci. U.S.A. **107**, 1301 (2010).
[10] G. Franzese, G. Malescio, A. Skibinsky, S. V. Buldyrev, and H. E. Stanley, Nature (London) **409**, 692 (2001).
[11] D. T. Limmer and D. Chandler, J. Chem. Phys. **135**, 134503 (2011).
[12] F. Sciortino, I. Saika-Voivod, and P. H. Poole, Phys. Chem. Chem. Phys. **13**, 19759 (2011).
[13] L. Liu, S. H. Chen, A. Faraone, C. W. Yen, and C. Y. Mou, Phys. Rev. Lett. **95**, 117802 (2005).
[14] A. K. Soper and M. A. Ricci, Phys. Rev. Lett. **84**, 2881 (2000).
[15] C. Huang, K. T. Wikfeldt, T. Tokushima, D. Nordlund, Y. Harada, U. Bergmann, M. Niebuhr, T. M. Weiss, Y. Horikawa, M. Leetmaa, M. P. Ljungberg, O. Takahashi, A. Lenz, L. Ojamae, A. P. Lyubartsev, S. Shin, L. G. M. Pettersson, and A. Nilsson, Proc. Natl. Acad. Sci. U.S.A. **106**, 15214 (2009).
[16] C. C. Huang, T. M. Weiss, D. Nordlund, K. T. Wikfeldt, L. G. M. Pettersson, and A. Nilsson, J. Chem. Phys. **133**, 134504 (2010).
[17] D. A. Fuentevilla and M. A. Anisimov, Phys. Rev. Lett. **97**, 195702 (2006).
[18] D. Banerjee, S. N. Bhat, S. V. Bhat, and D. Leporini, Proc. Natl. Acad. Sci. U.S.A. **106**, 11448 (2009).
[19] I. Brovchenko and A. Oleinikova, ChemPhysChem **9**, 2660 (2008).
[20] O. Mishima and Y. Suzuki, Nature (London) **419**, 599 (2002).
[21] M. D. Fayer and N. E. Levinger, Annu. Rev. Anal. Chem. **3**, 89 (2010).
[22] A. Faraone, K. H. Liu, C. Y. Mou, Y. Zhang, and S. H. Chen, J. Chem. Phys. **130**, 134512 (2009).
[23] A. Faraone, L. Liu, C. Y. Mou, C. W. Yen, and S. H. Chen, J. Chem. Phys. **121**, 10843 (2004).
[24] S. Klotz, T. Strassle, R. J. Nelmes, J. S. Loveday, G. Hamel, G. Rousse, B. Canny, J. C. Chervin, and A. M. Saitta, Phys. Rev. Lett. **94**, 025506 (2005).
[25] E. de la Llave, V. Molinero, and D. A. Scherlis, J. Chem. Phys. **133**, 034513 (2010).
[26] S. H. Chen, Y. Zhang, M. Lagi, S. H. Chong, P. Baglioni, and F. Mallamace, J. Phys.: Condens. Matter **21**, 504102 (2009).
[27] G. H. Findenegg, S. Jahnert, D. Akcakayiran, and A. Schreiber, ChemPhysChem **9**, 2651 (2008).
[28] L. D. Gelb, K. E. Gubbins, R. Radhakrishnan, and M. Sliwinska-Bartkowiak, Rep. Prog. Phys. **62**, 1573 (1999).
[29] N. Giovambattista, P. J. Rossky, and P. G. Debenedetti, J. Phys. Chem. B **113**, 13723 (2009).
[30] F. Mallamace, C. Branca, M. Broccio, C. Corsaro, C. Y. Mou, and S. H. Chen, Proc. Natl. Acad. Sci. U.S.A. **104**, 18387 (2007).
[31] F. Mallamace, M. Broccio, C. Corsaro, A. Faraone, D. Majolino, V. Venuti, L. Liu, C. Y. Mou, and S. H. Chen, Proc. Natl. Acad. Sci. U.S.A. **104**, 424 (2007).
[32] N. Giovambattista, P. J. Rossky, and P. G. Debenedetti, Phys. Rev. Lett. **102**, 050603 (2009).
[33] M. A. Ricci, F. Bruni, and A. Giuliani, Faraday Discuss. **141**, 347 (2009).
[34] S. H. Chen, L. Liu, E. Fratini, P. Baglioni, A. Faraone, and E. Mamontov, Proc. Natl. Acad. Sci. U.S.A. **103**, 9012 (2006).
[35] Y. Zhang, M. Lagi, E. Fratini, P. Baglioni, E. Mamontov, and S. H. Chen, Phys. Rev. E **79**, 040201 (2009).
[36] Y. Zhang, M. Lagi, F. Ridi, E. Fratini, P. Baglioni, E. Mamontov, and S. H. Chen, J. Phys.: Condens. Matter **20**, 502101 (2008).
[37] D. Z. Liu, Y. Zhang, C. C. Chen, C. Y. Mou, P. H. Poole, and S. H. Chen, Proc. Natl. Acad. Sci. U.S.A. **104**, 9570 (2007).
[38] Y. Zhang, A. Faraone, W. A. Kamitakahara, K. H. Liu, C. Y. Mou, J. B. Leao, S. Chang, and S. H. Chen, Proc. Natl. Acad. Sci. U.S.A. **108**, 12206 (2011).

This article is copyrighted as indicated in the abstract. Reuse of AIP content is subject to the terms at: http://scitation.aip.org/termsconditions. Downloaded to IP: 140.110.200.123 On: Mon, 25 Nov 2013 06:41:17

[39]Y. Zhang, K. H. Liu, M. Lagi, D. Liu, K. C. Littrell, C. Y. Mou, and S. H. Chen, J. Phys. Chem. B **113**, 5007 (2009).
[40]D. Z. Liu, Y. Zhang, Y. Liu, J. L. Wu, C. C. Chen, C. Y. Mou, and S. H. Chen, J. Phys. Chem. B **112**, 4309 (2008).
[41]Y. Zhang, A. Faraone, W. A. Kamitakahara, K. H. Liu, C. Y. Mou, J. B. Leao, S. Chang, and S. H. Chen, Proc. Natl. Acad. Sci. U.S.A. **108**, E1193 (2011).
[42]C. E. Bertrand, Y. Zhang, and S. H. Chen, Phys. Chem. Chem. Phys. **15**, 721 (2013).
[43]M. Erko, D. Wallacher, A. Hoell, T. Hauss, I. Zizak, and O. Paris, Phys. Chem. Chem. Phys. **14**, 3852 (2012).
[44]Y. Liu, W. Z. Zhang, and T. J. Pinnavaia, J. Am. Chem. Soc. **122**, 8791 (2000).
[45]L. Liu, S. H. Chen, A. Faraone, C. W. Yen, C. Y. Mou, A. I. Kolesnikov, E. Mamontov, and J. Leao, J. Phys.: Condens. Matter **18**, S2261 (2006).
[46]E. P. Barrett, L. G. Joyner, and P. P. Halenda, J. Am. Chem. Soc. **73**, 373 (1951).
[47]W. Thomson, Philos. Mag. **42**, 448 (1871).
[48]G. Halsey, J. Chem. Phys. **16**, 931 (1948).
[49]V. Velikov, S. Borick, and C. A. Angell, Science **294**, 2335 (2001).
[50]V. Alfredsson and M. W. Anderson, Chem. Mater. **8**, 1141 (1996).
[51]S. Kittaka, S. Ishimaru, M. Kuranishi, T. Matsuda, and T. Yamaguchi, Phys. Chem. Chem. Phys. **8**, 3223 (2006).
[52]S. Kittaka, Y. Ueda, F. Fujisaki, T. Iiyama, and T. Yamaguchi, Phys. Chem. Chem. Phys. **13**, 17222 (2011).
[53]S. Jahnert, F. V. Chavez, G. E. Schaumann, A. Schreiber, M. Schonhoff, and G. H. Findenegg, Phys. Chem. Chem. Phys. **10**, 6039 (2008).
[54]A. Schreiber, I. Ketelsen, and G. H. Findenegg, Phys. Chem. Chem. Phys. **3**, 1185 (2001).
[55]P. Gallo, M. A. Ricci, and M. Rovere, J. Chem. Phys. **116**, 342 (2002).
[56]S. Y. Xu, G. W. Scherer, T. S. Mahadevan, and S. H. Garofalini, Langmuir **25**, 5076 (2009).
[57]C. Hartnig, W. Witschel, E. Spohr, P. Gallo, A. Ricci, and M. Rovere, J. Mol. Liq. **85**, 127 (2000).
[58]S. H. Lee and P. J. Rossky, J. Chem. Phys. **100**, 3334 (1994).
[59]A. J. Patel, P. Varilly, and D. Chandler, J. Phys. Chem. B **114**, 1632 (2010).
[60]W. M. Ketcham and P. V. Hobbs, Philos. Mag. **19**, 1161 (1969).
[61]*CRC Handbook of Chemistry and Physics*, edited by W. M. Haynes (CRC Press, 2011), p. 6.
[62]C. A. Angell, R. D. Bressel, M. Hemmati, E. J. Sare, and J. C. Tucker, Phys. Chem. Chem. Phys. **2**, 1559 (2000).
[63]I. Brovchenko, A. Geiger, and A. Oleinikova, Phys. Chem. Chem. Phys. **3**, 1567 (2001).
[64]I. Brovchenko, A. Geiger, and A. Oleinikova, J. Chem. Phys. **118**, 9473 (2003).
[65]I. Brovchenko, A. Geiger, and A. Oleinikova, J. Chem. Phys. **123**, 044515 (2005).
[66]D. Paschek, Phys. Rev. Lett. **94**, 217802 (2005).
[67]P. H. Poole, F. Sciortino, U. Essmann, and H. E. Stanley, Nature (London) **360**, 324 (1992).
[68]R. Mancinelli, F. Bruni, and M. A. Ricci, J. Phys. Chem. Lett. **1**, 1277 (2010).
[69]A. K. Soper, Proc. Natl. Acad. Sci. U.S.A. **108**, E1192 (2011).
[70]A. K. Soper, J. Phys.: Condens. Matter **24**, 064107 (2012).
[71]F. Mallamace, M. Broccio, C. Corsaro, A. Faraone, U. Wanderlingh, L. Liu, C. Y. Mou, and S. H. Chen, J. Chem. Phys. **124**, 161102 (2006).
[72]S. H. Chen, F. Mallamace, C. Y. Mou, M. Broccio, C. Corsaro, A. Faraone, and L. Liu, Proc. Natl. Acad. Sci. U.S.A. **103**, 12974 (2006).
[73]L. M. Xu, P. Kumar, S. V. Buldyrev, S. H. Chen, P. H. Poole, F. Sciortino, and H. E. Stanley, Proc. Natl. Acad. Sci. U.S.A. **102**, 16558 (2005).

This article is copyrighted as indicated in the abstract. Reuse of AIP content is subject to the terms at: http://scitation.aip.org/termsconditions. Downloaded to IP: 140.110.200.123 On: Mon, 25 Nov 2013 06:41:17